Computational Investigation into Heteroleptic Photoredox Catalysts Based on Nickel(II) Tris-Pyridinethiolate for Water Splitting Reactions

Avik Bhattacharjee
Portland State University, bavik@pdx.edu

Dayalis S.V. Brown
Portland State University

Trent E. Ethridge
Portland State University

Kristine M. Halvorsen
Portland State University

Alejandra C. Acevedo Montano
Portland State University

Citation Details

Authors

Avik Bhattacharjee, Dayalis S.V. Brown, Trent E. Ethridge, Kristine M. Halvorsen, Alejandra C. Acevedo Montano, and Theresa M. McCormick

Article

Computational Investigation into Heteroleptic Photoredox Catalysts Based on Nickel(II) Tris-Pyridinethiolate for Water Splitting Reactions

Avik Bhattacharjee, Dayalis S. V. Brown, Trent E. Ethridge, Kristine M. Halvorsen, Alejandra C. Acevedo Montano, and Theresa M. McCormick*

Read Online

ACCESS | Metrics & More | Article Recommendations | Supporting Information

ABSTRACT: This work demonstrates a strategy to fine-tune the efficiency of a photoredox water splitting Ni(II) tris-pyridinethiolate catalyst through heteroleptic ligand design using computational investigation of the catalytic mechanism. Density functional theory (DFT) calculations, supported by topology analyses using quantum theory of atoms in molecules (QTAIM), show that the introduction of electron donating (ED) −CH$_3$ and electron withdrawing (EW) −CF$_3$ groups on the thiopyridyl (PyS$^-$) ligands of the same complex can tune the pK_a and E^0, simultaneously. Computational modeling of two heteroleptic nickel(II) tris-pyridinethiolate complexes with 2:1 and 1:2 ED and EW −CH$_3$

and −CF$_3$ group containing PyS$^-$ ligands, respectively, suggests that the ideal combination of EW to ED groups is 2:1. This work also outlines the possibility of formation of a large number of isomers after the protonation of one of the pyridyl N atoms and suggests that to acquire unambiguous computational results it is necessary to carefully account for all possible geometric isomers.

KEYWORDS: Water splitting, Photoredox catalyst, Heteroleptic catalyst design, DFT, QTAIM, Geometrical isomers, Intramolecular H-bonding
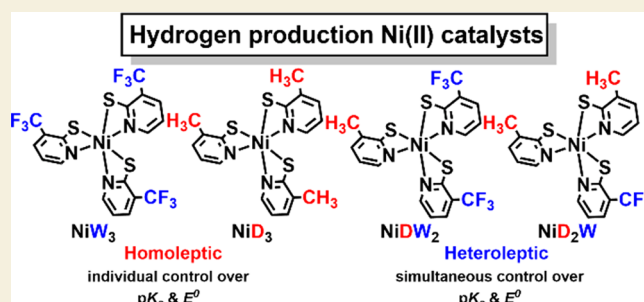
■ INTRODUCTION

Molecular hydrogen (H$_2$) is considered to be the fuel of the future to address the increasing global energy demand.[1,2] Although H$_2$ is a noncondensable gas at ambient temperature− pressure conditions with low volume energy density, it has the highest specific energy of combustion of all chemical fuels. The volume energy density exceeds all batteries, and burning H$_2$ does not lead to carbon emissions. H$_2$ can be accessed from the reductive side of the water splitting reactions through the reduction of aqueous protons in photochemical or electrochemical conditions.[3] As fascinating and simple as it might sound, producing molecular H$_2$ and O$_2$ from water in an experimental setup is extremely challenging due to the high overpotential associated with the reaction kinetics. It is for this reason that the involvement of a suitable catalyst is imperative to lower the overpotential of water splitting to allow the utilization of efficient photosensitizers in photoredox reactions.[4,5]

Due to lower overpotential for proton reduction, Pt and Pd complexes were most frequently studied as H$_2$ generation redox catalysts.[6] However, low abundance and higher cost of these metals limit the practical implementation of these catalysts, and interest has been shifted to the research of noble metal-free catalyst design for water splitting. Transition metal complexes containing Fe, Co, and Ni have been proven to be effective for water splitting.[7−16] The nickel(II) tris-pyridinethiolate, [Ni(PyS)$_3$]$^-$, catalyst has shown high efficiency in both photochemical and electrochemical systems.[8,17]

We have previously shown that H$_2$ production by [Ni(PyS)$_3$]$^-$ (1$^-$) follows a chemical−electrochemical−chemical− electrochemical (CECE) mechanism (Figure 1).[18] In the first step of the catalytic cycle, one of the three pyridyl N atoms is protonated and dechelates from the Ni(II) ion to form the protonated intermediate (1-H). The next step is an electron transfer to 1-H to form the reduced intermediate (1-H$^-$), followed by a proton coupled electron transfer (PCET) step to form a Ni−hydride intermediate (1-H$_2^-$). Finally, two H atoms come close to one another and leave the system as molecular H$_2$ gas to close the catalytic cycle (Figure 1).

In our previous work, we have shown that protonation of homoleptic 1$^-$ leads to the formation of four geometric
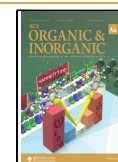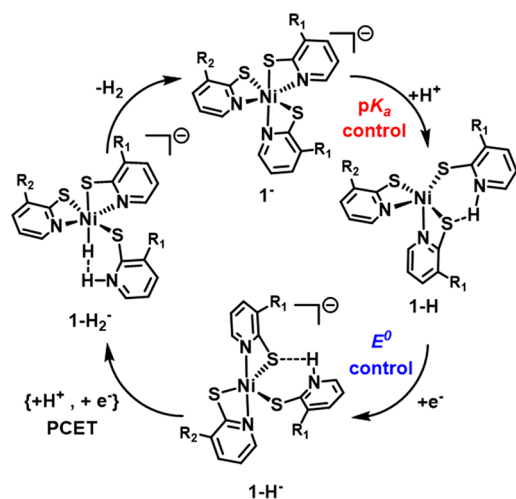
Figure 1. Catalytic cycle of H_2 production by heteroleptic Ni(II) tris-pyridinethiolate catalyst (1^-), where R_1 is either a $-CH_3$ or $-CF_3$ group, while R_2 is either a $-CF_3$ or $-CH_3$ group. The first step of the catalytic cycle (protonation of one of the three pyridyl N atoms and dechelation) is controlled by the pK_a, and the second step (reduction) is controlled by E^0. The protonation step can be optimized by introducing electron donating substituents while reduction can be tuned by installing electron withdrawing groups on the PyS$^-$ ligand.

isomers with different thermodynamic properties and stabilities due to the different basicities of the three pyridyl N atoms owing to the difference in the relative position around the Ni center afforded by a meridional geometry.[19] A topology analysis based on the quantum theory of atoms in molecules (QTAIM) on 12 homoleptic Ni(II) tris-pyridinethiolate catalysts supports that an intramolecular hydrogen bonding (H-bonding) interaction between the H$^+$ on the pyridyl N atom and an S atom from one of the neighboring thiopyridyl (PyS$^-$) ligands is responsible for the difference in the stabilities and properties of the isomers of protonated and reduced intermediates (Figure 1). We demonstrated that the H-bonding strength overcomes the thermodynamic *trans*-effect during the protonation of the catalysts and that these isomers should be considered in computational investigations of these types of catalysts.

We can surmise that the catalytic efficiency of 1^- is correlated with the ease of protonation and reduction. From a thermodynamic standpoint, better catalytic activity can be achieved by tuning the pK_a and E^0 of the original catalyst.[20] This can be attained by ligand modification. The pK_a of the catalyst can be increased by incorporating electron donating groups (EDGs) on PyS$^-$ ligands, enhancing the ability of the pyridyl N atoms to be protonated even at a higher pH conditions, while installing electron withdrawing groups (EWGs) on the aromatic rings will allow the E^0 value to be less negative, signifying the occurrence of a more spontaneous electrochemical step. Though it is necessary to modify the two thermodynamic parameters, pK_a and E^0, to optimize the catalytic activity of 1^-, these cannot be tuned simultaneously in a homoleptic catalyst. In this work, we propose the means to simultaneously optimize pK_a and E^0 through heteroleptic ligand modification of 1^-, meaning installing separate PyS$^-$ ligands with either electron donating (ED) or electron withdrawing (EW) groups on the same complex. We hypothesize that the ligands with EDG will tune the pK_a, while that with EWG will optimize the E^0 of the catalysts. To

investigate this hypothesis, we have computationally considered the catalytic mechanism of two heteroleptic Ni(II) tris-pyridinethiolate catalysts with 2:1 and 1:2 ratios of electron donating $-CH_3$ and electron withdrawing $-CF_3$ groups containing PyS$^-$ ligands and compared the results with the analogous homoleptic complexes (Figure 2).
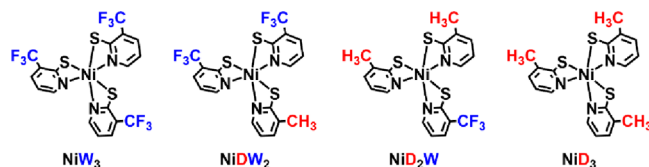
Figure 2. Heteroleptic catalysts studied in this work (**NiDW₂** and **NiD₂W**) and the analogous homoleptic catalysts (**NiW₃** and **NiD₃**) where **D** and **W** are the PyS$^-$ ligands containing electron donating $-CH_3$ and electron withdrawing $-CF_3$ groups at C-3 positions, respectively.

While modeling the heteroleptic starting catalysts (**NiDW₂** and **NiD₂W**), the possibility of isomer formation was considered on the basis of the location of the unique ligand (ligand with a stoichiometric ratio of one), and protonation of the pyridyl N of the **D** (electron donating) ligands generated a large number of protonated isomers. When modeling the reduction step, however, only the most thermodynamically stable protonated isomers were considered. The Ni−hydride intermediates formed after the proton-coupled electron transfer (PCET) step were modeled to gain insight on the relationship between the metal−hydride bond strength and electronic properties of the surrounding PyS$^-$ ligands. density functional theory (DFT) calculations assisted by topology analyses using QTAIM reveals the ideal configuration for the water splitting, heteroleptic $[Ni(PyS)_3]^-$ catalyst, is to have one **D** ligand controlling the protonation step while two **W** ligands lower the overpotential for reduction. The systematic approach of fine-tuning the catalytic efficiency of a well-known proton reduction catalyst through heteroleptic ligand modification described herein provides a strategy to optimize photocatalytic system components and can also be extrapolated to other related catalytic systems. The results described here mark the importance of considering the formation of isomers to support an explanation for unanticipated results while performing molecular modeling on structurally similar molecules in order to understand the mechanism in greater detail.

METHODS

The density functional theory (DFT) calculations were performed using the quantum chemistry package Gaussian 09 suite of programs.[21] The geometry optimization of the catalysts and catalytic intermediates was done using B3P86 functionals with 6-311+G(d,p) basis sets employing implicit water and acetonitrile solvation models. These solvents were chosen to match experimental reports where pK_a values are measured in water and E^0 values are measured in acetonitrile. No significant differences were observed using the different solvents. The frequency calculations were performed on the stationary points to extract the thermochemical energies. Gibbs energies for each intermediate were obtained using the sum of thermal and electronic energies resulted from the normal-mode frequency analyses. Single-point energy calculations were done using higher level of theories (M11-L and MP2) and the energies, compared against B3P86 to validate the method. The initial catalyst and protonated intermediates are in a triplet state, and the reduced intermediates are

in a doublet state, as previously determined.[18−20] Such calculation use unrestricted Kohn−Sham formalism.

The pK_a values were calculated by eq 1 using standard temperature and pressure conditions (298.15 K, 1 atm). The parametric value of the Gibbs energy of a water solvated proton (−264 kcal mol$^{−1}$) was used to calculate the free energy change of the protonation step as described by eq 2.[22−26]

$$pK_a = -\frac{\Delta G^0_{rxn}}{RT \ln 10} \tag{1}$$

$$\Delta G^0_{rxn} = G_{[R]1-H} - (G_{1-} - 264) \tag{2}$$

The reduction potential (E^0) values were calculated using the principle of isodesmic reactions. The experimental reduction potential of the parent $[\mathbf{Ni(PyS)_3}]\mathbf{H}/[\mathbf{Ni(PyS)_3}]\mathbf{H}^-$ couple of −1.62 V vs SCE was used as a reference (E^0_{ref}) in eq 3.[20]

$$E^0 = -\frac{\Delta G^0}{F} + E^0_{ref} \tag{3}$$

The relative population (x) of the protonated isomers was calculated by employing the Boltzmann population distribution formula (eq 4) at 298.15 K and normalized to unity with respect to the most stable isomer, assuming the population was only determined by the thermodynamic stability.[27]

$$x = \frac{\exp(-\Delta G^0_i / RT)}{\sum_i \exp(-\Delta G^0_i / RT)} \tag{4}$$

The structural parameters such as bond lengths and bond angles of the optimized structures of the catalytic intermediates were determined using the GaussView 5.0 visualization software.[28]

The intramolecular H-bonds were investigated through the topological analysis of the electron density distribution using quantum theory of atoms and molecules (QTAIM).[29−31] Wave function files of the optimized structures generated by Gaussian 09 were analyzed using Multiwfn 3.7 package.[32] The bond energies of the H-bonds (BEs in kcal mol$^{−1}$) were calculated from the electron densities (ρ's) at the bond critical points (BCPs) employing eq 5.[33,34] The reported error on the QTAIM method for determining hydrogen bond strength is 14.7%.[34]

$$BE \approx -223.08 \times \rho + 0.7423 \tag{5}$$

RESULTS AND DISCUSSION

Isomers of the Heteroleptic Starting Catalysts

The unsubstituted homoleptic Ni(II) tris-pyridinethiolate catalyst adopts a pseudo-octahedral geometry where the three bidentate PyS$^−$ ligands are oriented in a meridional (mer) fashion around the Ni(II) center.[19] This geometry is supported by X-ray crystallography.[17] The computational modeling of these compounds in both mer and fac configurations shows the corresponding mer isomers are lower in energy. The mer geometry results in different chemical environments and thus different basicities of the three pyridyl N atoms owing to the difference in their relative position. We have developed a scheme and naming convention to distinguish between the N atoms based on an imaginary meridional plane containing the three pyridinethiolate S atoms (Figure 3). The N atom contained by the plane of the S atoms is $\mathbf{N[C]}$, and the N atoms to the right and left side of the plane are $\mathbf{N[R]}$ and $\mathbf{N[L]}$, respectively.

DFT calculations on the heteroleptic $\mathbf{NiDW_2}$ and $\mathbf{NiD_2W}$ have revealed that mer orientation of the ligands around the Ni(II) center is preferred thermodynamically over the fac isomers, similar to the homoleptic compounds,[18,19] but unlike the homoleptic complexes, three isomers of the starting
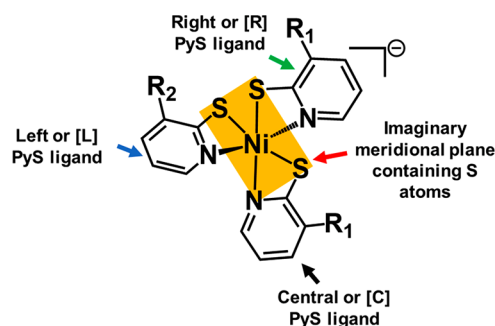
Figure 3. Identifying the different pyridyl N atoms based on their relative position with respect to the imaginary meridional plane containing the three S atoms (yellow plane), where R$_1$ is either a −CH$_3$ or −CF$_3$ group and R$_2$ is either a −CF$_3$ or −CH$_3$ group. The meridional plane contains a [C] N atom, while [L] and [R] N atoms are to the left and right side of the plane, respectively. The position of the unique ligand with respect to the meridional plane determines the identity of the isomer of the catalyst. The PyS$^−$ ligand containing R$_2$ group is placed on the left side of the meridional plane making it an [L] isomer.

catalysts are possible for each heteroleptic compound based on the position of the unique ligand prior to protonation. This is because the unique ligand can be introduced to any of the three PyS$^−$ ligand positions. For example, heteroleptic $\mathbf{NiDW_2}$ contains $\mathbf{W}$ ligands with an EW −CF$_3$ group and $\mathbf{D}$ ligand with an ED −CH$_3$ group in a ratio of 2:1. Hence, in case of $\mathbf{NiDW_2}$, $\mathbf{D}$ ligand is the unique ligand and the position of $\mathbf{D}$ ligand relative to the meridional plane of S atoms outlined above will dictate the name of the isomer. If the $\mathbf{D}$ ligand is in the center and contained within the plane of the S atoms, the isomer will be called [C] $\mathbf{NiDW_2}$, and if the $\mathbf{D}$ ligand is placed on the right or left side of the imaginary plane of S atoms, it will be called [R] $\mathbf{NiDW_2}$ or [L] $\mathbf{NiDW_2}$, respectively (Figure 4a). Similarly,
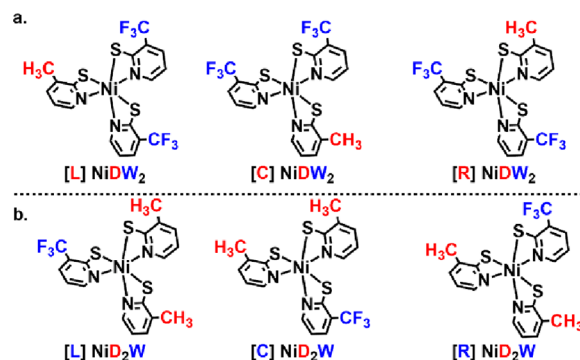
Figure 4. Possible isomers of the starting catalysts based on the relative position of the unique ligands in the case of heteroleptic complexes.

in case of $\mathbf{NiD_2W}$, the unique ligand is $\mathbf{W}$ (a PyS$^−$ ligand containing an EW −CF$_3$ group); hence, the position of the $\mathbf{W}$ ligand with respect to the meridional plane containing three S atoms will dictate the names of the isomers, such as [C] $\mathbf{NiD_2W}$, [L] $\mathbf{NiD_2W}$, and [R] $\mathbf{NiD_2W}$ when the $\mathbf{W}$ ligand is placed on, to the left side, and to the right side of the plane, respectively (Figure 4b).

Boltzmann population distributions of these isomers were calculated from the optimized geometries using the thermodynamic energies, and as anticipated, the contribution from each isomer was ~33% (Table 1). The uniform population

Table 1. Calculated Boltzmann Population Distribution (% x) and the ΔG and ΔH Values Used to Calculate Them for the Isomers of the Starting Heteroleptic Catalysts at Room Temperature[a]

heteroleptic complex	isomer of the starting catalyst	ΔH (kcal mol^{-1})	ΔG (kcal mol^{-1})	Boltzmann population (% x)
NiDW$_2$	[**C**]	0.004	0.012	33.9
	[**L**]			34.5
	[**R**]	0.043	0.053	31.6
NiD$_2$W	[**C**]			34.0
	[**L**]	0.004	0.004	33.7
	[**R**]	0.034	0.030	32.3

[a]The most stable isomer was used as the reference.

distribution of these isomers suggest that the thermodynamic properties and stabilities of these complexes are very similar; therefore when synthesized, it is reasonable to expect an equimolar mixture of the three isomers.

Effect of Ligand Modification on the pK_a

To investigate the role of ligand modification on the protonation of the catalysts, we have modeled all possible protonated isomers of the heteroleptic **NiDW$_2$** and **NiD$_2$W** by protonating the pyridyl N atoms of the **D** ligands separately. We hypothesize that the ED −CH$_3$ group containing **D** ligands will be preferentially protonated over the EW −CF$_3$ group containing **W** PyS$^-$ ligands. This was supported by calculating and comparing the Boltzmann populations of **D** and **W** protonated ligands. The Boltzmann population analysis is determined on the basis of the calculated thermodynamic differences in energies of the isomers. Intrinsic error in the energy calculations is accepted to be 2 kcal/mol for this method; when one considers this, these values may be off by up to ±2%. However, since the compounds are structurally so similar, one would expect a similar error in each compound. Caution should also be taken in interpreting these values since kinetic factors were not considered. The relative population of the complexes were negligible when protonation of **W** ligands was considered compared to the most stable isomers generated through the protonation of **D** ligands (Tables S1 and S2). In our previous work, we have shown that the protonation of the pyridyl N atoms are guided by the formation of intramolecular H-bonding with one of the adjacent thiopyridyl S atoms and not on the thermodynamic trans effect.[19] The stability of the protonated isomers is directly proportional to the H-bond strength. The existence of similar intramolecular H-bonding interactions was also observed for these protonated heteroleptic complexes. Hence, to justify the difference and population of the protonated heteroleptic isomers, the H-bond strengths were calculated from the topology analyses of the electron densities using QTAIM.

Protonation of NiDW$_2$ Complex

The heteroleptic **NiDW$_2$** catalyst has only one protonation site at **D**, the unique ligand. Therefore, the **D** ligands of all the three isomers of the starting catalysts [**C**] **NiDW$_2$**, [**L**] **NiDW$_2$**, and [**R**] **NiDW$_2$** were separately protonated. As mentioned earlier, protonated intermediates involve an intramolecular H-bonding interaction where the protonated N atom is the H-bond donor and one of the adjacent thiopyridyl S atoms is the H-bond acceptor. This leads to the formation of *six* possible protonated isomers (Figure 5). We have named these such that the first letter denotes the location of the unique ligand, the
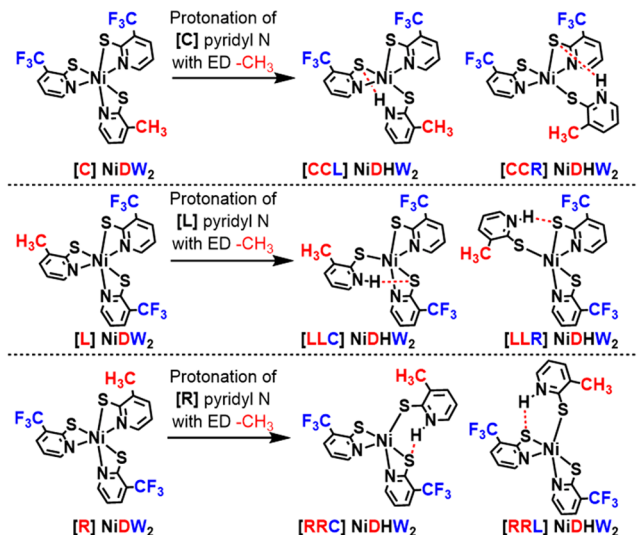
Figure 5. Protonation of the unique **D** ligands of the three isomers of **NiDW$_2$** starting catalysts to generate six possible protonated isomers. The intramolecular H-bonding interactions between pyridyl N−H and one of the adjacent thiopyridyl S atoms are shown using red dashed bonds.

second letter denotes the location of the protonated N, and the third letter denotes the ligand H-bonding to the proton. For example, the protonation of [**C**] **NiDW$_2$** forms [**CCL**] **NiDHW$_2$**, where the protonated [**C**] pyridyl N atom is the H-bond donor and the adjacent [**L**] thiopyridyl S atom is the H-bond acceptor, and [**CCR**] **NiDHW$_2$**, where the protonated [**C**] pyridyl N atom is the H-bond donor and the adjacent [**R**] thiopyridyl S atom is the H-bond acceptor, while protonation of [**L**] **NiDW$_2$** leads to [**LLC**] **NiDHW$_2$** and [**LLR**] **NiDHW$_2$**, where the [**L**] pyridyl N atom is the H-bond donor in both cases but [**C**] thiopyridyl S and [**R**] thiopyridyl S atoms act as H-bond acceptors, respectively. Similarly, in the case of protonated isomers [**RRC**] **NiDHW$_2$** and [**RRL**] **NiDHW$_2$**, protonated [**R**] pyridyl N is the H-bond donor and [**C**] and [**L**] thiopyridyl S are H-bond acceptors, respectively.

DFT calculations on these six protonated isomers followed by topology analyses have revealed that [**CCL**] and [**CCR**] are the same molecules with the same thermodynamic energies and intramolecular H-bond strength, collectively referred to as [**C**] **NiDHW$_2$**. Similarly, protonation of [**R**] **NiDW$_2$** leads to only one protonated intermediate, as [**RRC**] and [**RRL**] have the same thermodynamic energies. Conversely, protonation of the [**L**] pyridyl N atom of [**L**] **NiDW$_2$** forms two isomers, [**LLC**] and [**LLR**], on the basis of the identity of the H-bond acceptor thiopyridyl S atoms. This reduces the total number of the protonated isomers of **NiDHW$_2$** catalyst to four (Figure 6). Of these four isomers, [**R**] **NiDW$_2$** is the most thermodynamically stable. On the basis of the thermodynamic stabilities, we calculated the expected population distribution under standard conditions (Table 2). To investigate the origin of the unequal relative population distribution of the isomers of the protonated **NiDW$_2$** heteroleptic complexes, we used topology analyses. The electron density distribution of the H-bonded network in these isomers using QTAIM enabled us to correlate the strength of these bonds with the relative thermodynamic stabilities (Table 2). As anticipated, the most thermodynamically stable [**R**] isomer of **NiDHW$_2$** (65.2%) forms the strongest intramolecular H-bonded network (−6.51 kcal
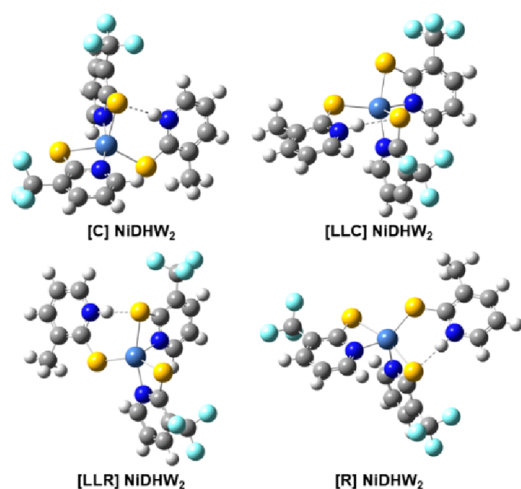
Figure 6. Ball and stick structures of the optimized protonated isomers of **NiDHW$_2$** where blue, gray, yellow, white, indigo, and cyan balls represent N, C, S, H, Ni, and F atoms, respectively. The intramolecular H-bonding interactions (N−H···S) are shown using dashed bonds.

mol^{-1}), and the least stable [**C**] isomer (3.8%) forms the weakest intramolecular H-bond (−5.14 kcal mol^{-1}) with the neighboring thiopyridyl S atom (Figure S1).

Protonation of NiD$_2$W Complexes

The protonation of the heteroleptic **NiD$_2$W** complex is more complicated as it contains more than one −CH$_3$ group containing **D** ligands. We hypothesize that the protonation of the **NiD$_2$W** complex could lead to the formation of up to 12 isomers on the basis of the identity of the protonated **D** ligand and the identity of the H-bonded S atom from one of the adjacent PyS$^-$ ligands (Scheme 1). All 12 complexes were modeled using DFT by separately protonating each of the **D** ligands. As observed in the case of protonated isomers of **NiDW$_2$**, the isomers of **NiD$_2$HW** were of different thermodynamic stabilities. The intramolecular H-bonded structures were studied using QTAIM based topology analyses to correlate the strength of H-bonds with the relative population of the isomers (Figures 7 and S2). When compared among three different levels of theories, namely, B3P86, M11-L, and MP2, the trends in the energy differences among the protonated isomers were found to be consistent. For example, for **NiDHW$_2$**, the most stable isomer for all three levels of theory was found to be the [**R**] isomer with the Boltzmann population distribution for this isomer being 72% for B3P86, 70% for M11-L, and 76% for MP2, indicating that the trends are exclusive of the choice of the functional (Table S3). The remaining calculations were exclusively done with B3P86 level of theory to be consistent with previous computational studies on this class of compounds.[18−20]

The DFT studies supported by QTAIM based topology analyses reveals that protonation of the **D** ligands of three isomers of the starting catalysts form eight different isomers instead of the originally predicted twelve (Scheme 2, Figure S3). Isomers are formed as pairs with the exact same thermodynamic stabilities and H-bond strength; e.g., [**CRC**] and [**LRL**] are the same molecules. Similarly, [**CRL**] and [**LRC**], [**RCL**] and [**LCR**], and finally, [**RCR**] and [**LCL**] are identical molecules with the same thermodynamic energies. However, [**CLC**], [**CLR**], [**RLC**], and [**RLR**] isomers of **NiD$_2$HW** are unique isomers with no structural conjugates. In summary, protonation of the [**L**] isomer of the starting **NiD$_2$W** catalyst leads to four isomers that are structurally identical with four other isomers formed through protonation of either [**C**] or [**R**]. Hence, only *eight* isomers formed by protonation of [**C**] and [**R**] isomers of **NiD$_2$WH** will be discussed and are referred to as [**CLC**], [**CLR**], [**CRC**], [**CRL**], [**RCL**], [**RCR**], [**RLC**], and [**RLR**]. These isomers vary in terms of their relative population. The Boltzmann populations were compared with the intramolecular N−H···S H-bond strengths (Table 3). These results deviated somewhat from the original hypothesis that the unequal population distribution can be explained solely on the basis of the strength of these intramolecular H-bonds. For example, the most stable [**CRL**] protonated isomer (49.4%) has lower H-bond stabilization (−6.97 kcal mol^{-1}) when compared to the [**CRC**] isomer (−7.48 kcal mol^{-1}), which has a lower Boltzmann population (20.4%). However, when these H-bonds strengths were plotted against the quantum mechanically derived single point energies, an overall linear correlation was observed (Figure S4).

In order to further refine the hypothesis to justify the unequal Boltzmann distribution of the protonated intermediates, a closer inspection of the metal−ligand framework was performed. The penta-coordinated square pyramidal protonated isomers can be broadly classified into two categories: (a) S atom capped square pyramids and (b) N atom capped square pyramids. N-capped square pyramids were consistently thermodynamically more stable when compared with the S-capped square pyramids (Figure 8). This can possibly be attributed to a lower steric interaction between the bulky S atoms in the N-capped square pyramidal configuration. Thus, the stability trends with the structural differences in these complexes, which will dictate the calculated pK_a values.

pK_a Values of the Complexes

The pK_a values of all possible isomers of the protonated complexes were calculated (Table S4). It has been observed that for a single compound the distribution in the pK_a values is 1.3 and 4 pK_a units for **NiDW$_2$** and **NiD$_2$W** complexes, respectively. The calculated pK_a values of the most stable protonated isomers of **NiDHW$_2$** ([**R**]) and **NiD$_2$HW** ([**CRL**]) were compared to the homoleptic analogues **NiW$_3$** and **NiD$_3$**

Table 2. Comparison of the Intramolecular H-Bond Stabilization Energy (kcal mol^{-1}) with the Boltzmann Distribution (% x) and the ΔG and ΔH Values Used to Calculate Them for the Isomers of the Protonated Intermediates for NiDW$_2$^{a}

protonated heteroleptic complex	isomers	ΔH (kcal mol^{-1})	ΔG (kcal mol^{-1})	Boltzmann population (% x)	N−H···S BE (kcal mol^{-1})
NiDHW$_2$	[**C**]	1.68	1.69	3.76	−5.14
	[**LLC**]	2.01	1.55	4.73	−5.33
	[**LLR**]	0.76	0.54	26.3	−6.44
	[**R**]			65.2	−6.51

^{a}Isomer [**R**] is the most stable and was used as the reference.

Scheme 1. Nomenclature of the Protonated Isomers Generated from the NiD$_2$W Heteroleptic Complexes[a]

Heteroleptic complex	Unique W ligand	Protonated D ligand	S atom of adjacent PyS$^-$ ligand	Protonated isomer
NiD$_2$HW	[C]	[L]	[C]	**[CLC]**
			[R]	**[CLR]**
		[R]	[C]	**[CRC]**
			[L]	**[CRL]**
	[L]	[C]	[L]	**[LCL]**
			[R]	**[LCR]**
		[R]	[C]	**[LRC]**
			[L]	**[LRL]**
	[R]	[C]	[L]	**[RCL]**
			[R]	**[RCR]**
		[L]	[C]	**[RLC]**
			[R]	**[RLR]**

[a]Considers the intramolecular H-bonding network where the pyridyl N atom from one of the **D** ligands acts as a H-bond donor and an S atom from one of the adjacent PyS$^-$ ligands behaves as the H-bond acceptor.
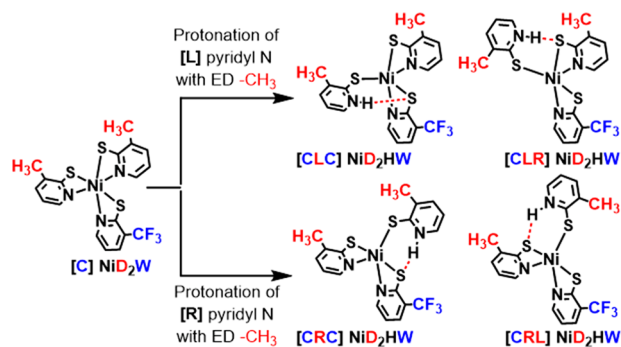
Figure 7. Four isomers of [C] **NiD$_2$HW** complexes considering protonation of both [L] and [R] ligands and intramolecular H-bonded networks with the adjacent PyS$^-$ ligands through the S atoms separately. The intramolecular H-bonding interactions are shown using red dashed bonds.

Scheme 2. Protonation of Three Starting Isomers of NiD$_2$W Catalysts Produces Eight Isomers Instead of the Originally Proposed 12 Isomers
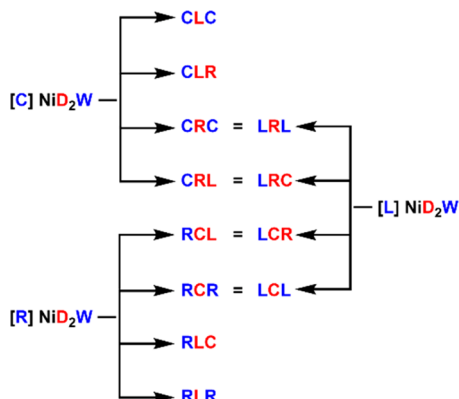
(Table 4). An increase in the pK$_a$ of the catalysts is observed with an increasing the number of electron donating **D** ligands. It is possible to achieve better control over the basicity of the pyridyl N atoms through the incorporation of ED substituents in the ligand framework as hypothesized earlier. The tunability ranges from 8.5 to 12.7 pK$_a$ units with zero to three **D** ligands, respectively, and as anticipated, the pK$_a$ values of the

heteroleptic complexes are intermediate between their homoleptic analogues.

Effect of Ligand Modification on E^0

The reduction step of the most stable protonated isomers was modeled by adding an extra electron to the system in an implicit acetonitrile solvation model. The reduction of **NiDHW$_2$** leads to the formation of **NiDHW$_2^-$**, while the reduction of **NiD$_2$HW** generates **NiD$_2$HW$^-$** (Figure 9). The reduction step changes the oxidation state of the central metal ion from +2 to +1. The ligand coordination around the Ni center also changes from a square pyramid to a trigonal bipyramid. The structural changes were investigated by calculating the structure index parameter (τ) value of the metal−ligand framework as introduced by Addison et al.,[35] where for an ideal trigonal bipyramid, τ is 1 and an ideal square pyramid τ is 0 (Figure S5).[36] In the case of the reduced complexes, τ values are 0.7 and 0.76 for **NiDHW$_2^-$** and **NiD$_2$HW$^-$**, respectively (Table S5), indicating a trigonal bipyramid structure. The reduction potential values (E^0) were calculated from the Gibbs energy change of these one-electron reduction events using the concept of isodesmic reactions (Table 4). A balanced reaction is created assuming an internal electron transfer from a reference reduction reaction with a known reduction potential. The reduction potential of the unsubstituted ($[Ni(PyS)_3H]^-/[Ni(PyS)_3H]$) couple, −1.62 V vs SCE, was used as the reference value (E_{ref}^0).[19,20]

In general, more electron withdrawing ligands result in less negative reduction potentials. When compared with the homoleptic analogue **NiD$_3$**, the E^0 values of the heteroleptic catalysts increase to more positive values with the increase in the number of EW **W** ligands, accounting for a more spontaneous reduction process. However, when **NiW$_3$** is compared with **NiDW$_2$**, the latter is slightly easier to reduce even though the former has more **W** ligands. This can be attributed to the difference in the extent of stabilities of the protonated intermediates of **NiW$_3$H** and **NiDHW$_2$**. Since the method of calculation of E^0 values using isodesmic reactions utilizes the free energies of both protonated and reduced intermediates and further compares it with the reference reaction of the unsubstituted nickel tris-pyridinethiolate catalysts, the comparison of the free energy change of the reaction is more appropriate than comparing the absolute value of E^0 calculated by the employment of this method.

Table 3. Comparison of the Intramolecular H-Bond Stabilization Energy (kcal mol^{-1}) with the Boltzmann Distribution (% x) and the ΔG and ΔH Values Used to Calculate Them for the Isomers of the Protonated Intermediates for NiD$_2$W[a]

protonated heteroleptic complex	isomers	ΔH (kcal mol^{-1})	ΔG (kcal mol^{-1})	Boltzmann population (% x)	N–H···S BE (kcal mol^{-1})
NiD$_2$HW	[CLC]	2.76	2.00	2.51	−5.19
	[CLR]	6.05	5.53	7.94	−7.02
	[CRC]	0.76	0.53	20.4	−7.48
	[CRL]			49.4	−6.97
	[RCL]	1.62	1.06	8.27	−5.81
	[RCR]	2.39	2.51	0.72	−5.82
	[RLC]	1.83	1.76	2.51	−5.66
	[RLR]	1.42	1.13	8.27	−6.60

[a]Isomer [CLR] is the most stable and was used as the reference.
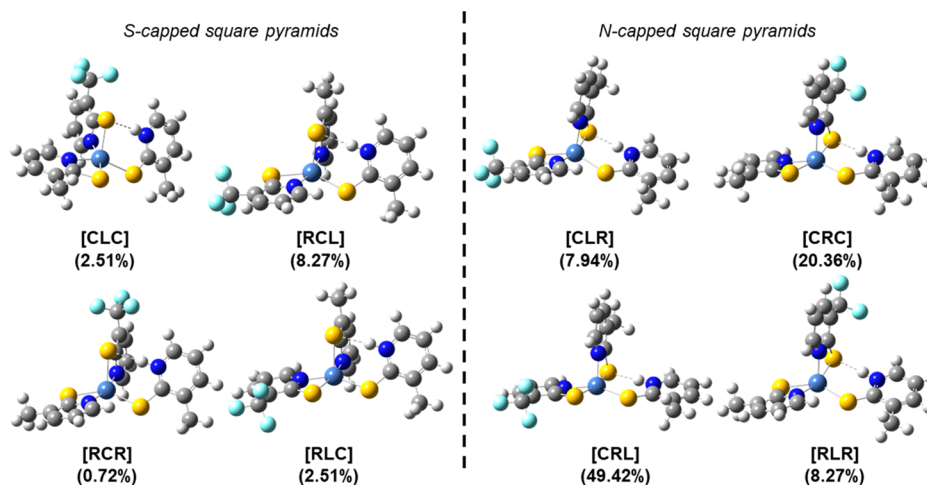
Figure 8. Ball and stick structures of the optimized protonated isomers of **NiD$_2$HW** including relative Boltzmann populations, classified in two groups: S-capped and N-capped square pyramidal complexes. The blue, gray, yellow, white, indigo, and cyan balls represent N, C, S, H, Ni, and F atoms, respectively. The intramolecular H-bonding interactions (N–H···S) are shown using dashed bonds.

Table 4. Calculated pK_a of the Thermodynamically Most Stable Protonated Isomers in an Implicit Water Solvation Model and the Calculated E^0 Values in an Implicit Acetonitrile Solvation Model of the Reduced Isomers of the Heteroleptic Complexes and Comparison with the Homoleptic Analogues at Room Temperature

catalysts	most stable protonated isomer	calculated pK_a values	calculated E^0 V vs SCE
NiW$_3$		8.5	−1.44
NiDW$_2$	[R]	9.5	−1.40
NiD$_2$W	[CRL]	11.1	−1.53
NiD$_3$		12.7	−1.69

Figure 9. Ball and stick structures of the optimized reduced intermediates: **NiDHW$_2^-$** and **NiD$_2$HW$^-$**. The modified PyS$^-$ ligands are oriented in a trigonal bipyramidal fashion around the Ni(I) metal cation. The blue, gray, yellow, white, indigo, and cyan balls represent N, C, S, H, Ni, and F atoms, respectively.

Effect of Ligand Modification on the Hydride Intermediates

The final step of the catalytic cycle of water splitting using nickel(II) tris-pyridinethiolates is a proton coupled electron transfer (PCET) resulting in a Ni(0)−hydride intermediate.[18] This is modeled by adding a proton and electron to the reduced complex. Consequently, the nickel center regains an octahedral coordination. The hydride attached to Ni(0) and the proton on the pyridyl N atom are near enough to each other to allow for a hydrogen molecule to be released, reforming the original catalyst. The PCET intermediates of the heteroleptic catalysts **NiDH$_2$W$_2^-$** and **NiD$_2$H$_2$W$^-$** were modeled in an acetonitrile implicit solvation model (Figure 10). The structural parameters corresponding to H···H

interactions were measured along with the Gibbs energy change for the hydrogen release reactions for the heteroleptic complexes along with their homoleptic analogues (Table 5).

The similarities in the structural parameters of the Ni(0)−hydride intermediates of the homoleptic and heteroleptic complexes indicate that ligand modification has little to no effect on the final two steps of the catalytic cycle of hydrogen production using Ni(II) tris-pyridinethiolates. The free energy changes of the hydrogen evolution reactions are very similar for all four compounds. This observation indicates that tuning the catalytic efficiency of the proton reduction Ni(II) tris-
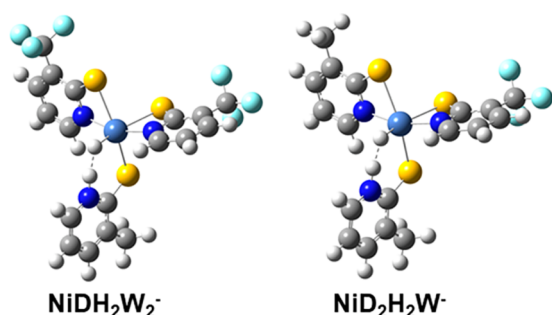
Figure 10. Ball and stick structures of the optimized metal−hydride intermediates in the acetonitrile implicit solvation model: $NiDH_2W_2^-$ and $NiD_2H_2W^-$. The blue, gray, yellow, white, indigo, and cyan balls represent N, C, S, H, Ni, and F atoms, respectively. The interactions between the two H atoms (H···H) trapped between the Ni and a pyridyl N atom are shown using dashed bonds.

Table 5. Structural Parameters of the PCET Intermediates of the Heteroleptic and Homoleptic Catalysts and the Free Energy Change of the Hydrogen Release Step to Regain the Original Configuration at Room Temperature

PCET intermediate	N−H bond length (Å)	Ni−H bond length (Å)	H···H bond length (Å)	Gibbs energy change for H₂ release (kcal mol⁻¹)
$NiW_3H_2^-$	1.09	1.64	1.35	−28.7
$NiDH_2W_2^-$	1.07	1.64	1.41	−26.3
$NiD_2H_2W^-$	1.07	1.64	1.40	−25.8
$NiD_3H_2^-$	1.07	1.64	1.40	−26.5

pyridinethiolate catalysts are appropriately modeled targeting the first two steps of the catalytic cycle. The energetics of the full catalytic cycle were compared for the heteroleptic complexes in an acetonitrile solvation model at a solution pH of 12.1 and under an applied electrochemical potential of −1.62 V vs SCE, which are the experimentally observed pK_a and reduction potential value of the unsubstituted homoleptic Ni(II) tris-pyridinethiolate catalyst (Figure 11). The parametric values of an acetonitrile solvated proton (−260.2 kcal

mol⁻¹) and electron (−31.9 kcal mol⁻¹) were used to calculate the free energy change (ΔG), enthalpy change (ΔH), and entropy change (ΔS) of the individual catalytic steps (Table S6).[37−40] Protonation of more EDG containing NiD_2W is 3.8 kcal mol⁻¹ more favorable, while reduction of more EWG containing $NiDW_2$ is more favorable by 2.9 kcal mol⁻¹ at room temperature. From the calculated thermodynamic energies, it is observed that the Ni(0)−hydride intermediates have similar energies (within 0.3 kcal mol⁻¹). However, since the reduced intermediate of $NiDW_2$ is more stable than NiD_2W, the PCET step of $NiDW_2$ is less energy demanding than NiD_2W. Finally, the hydrogen evolution step requires similar energy for both heteroleptic complexes. On the basis of these calculations of the thermodynamic parameters, it can be concluded that the ideal combination for the heteroleptic catalyst for proton reduction by Ni(II) tris-pyridinethiolate would be to have one ligand containing an electron donating group (**D**) that will tune the pK_a value of the complex and two electron withdrawing ligands (**W**) to tune the E^0 value of the complex toward a more positive value leading to a more spontaneous reduction process.

■ CONCLUSIONS

This work provides computational insight into tuning the catalytic efficiency of proton reduction Ni(II) tris-pyridine-thiolate photoredox catalysts through heteroleptic ligand design. The previously reported catalytic cycle outlines the role of pK_a and E^0, which need to be simultaneously optimized in order to tune the catalytic efficiency. The introduction of ED groups accounts for a higher pK_a; however, a less negative E^0 requires EW groups. Since these two properties require two opposing ligand modifications, a heteroleptic catalyst containing both ED and EW groups in a single complex can modulate both the thermodynamic properties. To test the hypothesis, two heteroleptic complexes $NiDW_2$ and NiD_2W were studied, and the calculated thermodynamic parameters were compared with the corresponding homoleptic analogues (NiW_3 and NiD_3). DFT calculations along with QTAIM results indicate that the ideal configuration for the heteroleptic catalyst design for water splitting reactions is $NiDW_2$, where one ED **D** ligand
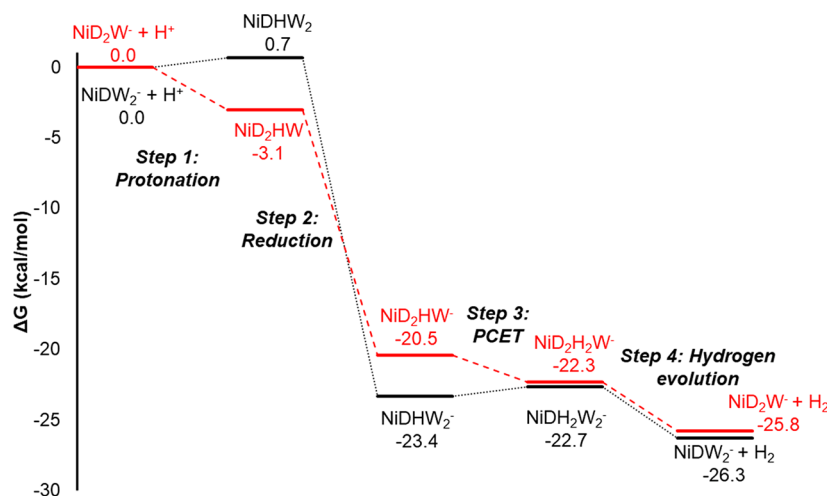
Figure 11. Energy profile diagram corresponding to the catalytic steps of proton reduction using $NiDW_2$ and NiD_2W heteroleptic complexes calculated at a solution pH of 12.1 and under an applied electrochemical potential of −1.62 V vs SCE. Thermodynamically, most stable geometric isomers in these conditions are considered for this plot. The free energy changes are reported in kcal mol⁻¹. The presence of more D ligands accounts for an easier protonation, while more W ligands make the reduction step more spontaneous, characterized by a higher free energy change.

tunes the pK_a to a higher value and two EW **W** ligands contribute to a more favorable reduction process.

It was observed previously that the catalytic mechanism of the homoleptic $[\mathbf{Ni(PyS)_3}]^-$ proceeds through the protonation of one of the pyridyl N atoms. Due to the asymmetric ligand environment around the Ni center, protonation leads to the formation of geometric isomers. The stability of these isomers is related to the strength of an intramolecular H-bonding interaction between the pyridyl N—H and one of the adjacent thiopyridyl S atoms. In the case of heteroleptic complexes, isomer formation through protonation was also observed, and due to higher structural complexity in the heteroleptic complexes, the number of isomers is much higher than that in the homoleptic analogues. This work demonstrates the importance of carefully accounting for contributions from all of the isomers while computationally modeling structurally intricate systems in order to achieve unambiguous and meaningful results. In summary, this report shows that the introduction of the ED $-CH_3$ group in the ligand environment of the heteroleptic complexes systematically increases the pK_a. Conversely, EW $-CF_3$ groups make the E^0 more positive when compared with their homoleptic analogues.

■ ASSOCIATED CONTENT

ⓢ Supporting Information

The Supporting Information is available free of charge at https://pubs.acs.org/doi/10.1021/acsorginorgau.2c00040.

Isomer population tables, total calculated energies, topology maps of the isomers, index parameter values, and thermodynamic parameters in solvent (PDF)

xyz coordinates of the optimized structures (XYZ)

■ AUTHOR INFORMATION

Corresponding Author

Theresa M. McCormick — *Portland State University, College of Liberal Arts & Sciences, Department of Chemistry, Portland, Oregon 97207, United States;* ⓞ orcid.org/0000-0003-1745-2911; Email: t.m.mccormick@pdx.edu

Authors

Avik Bhattacharjee — *Portland State University, College of Liberal Arts & Sciences, Department of Chemistry, Portland, Oregon 97207, United States;* Present Address: Department of Chemistry, York University, Chemistry Building 450, 4700 Keele St, Toronto, Ontario M3J 1P3, Canada

Dayalis S. V. Brown — *Portland State University, College of Liberal Arts & Sciences, Department of Chemistry, Portland, Oregon 97207, United States*

Trent E. Ethridge — *Portland State University, College of Liberal Arts & Sciences, Department of Chemistry, Portland, Oregon 97207, United States*

Kristine M. Halvorsen — *Portland State University, College of Liberal Arts & Sciences, Department of Chemistry, Portland, Oregon 97207, United States;* Present Address: Norwegian University of Science and Technology Postboks 8900, NO-7491 Trondheim, Torgarden, Norway; ⓞ orcid.org/0000-0002-3172-7558

Alejandra C. Acevedo Montano — *Portland State University, College of Liberal Arts & Sciences, Department of Chemistry, Portland, Oregon 97207, United States;* Present Address: Department of Chemistry, Smith Hall, 207

Pleasant St SE, Minneapolis, Minnesota 55455-0431, United States

Complete contact information is available at: https://pubs.acs.org/10.1021/acsorginorgau.2c00040

Author Contributions

CRediT: **Avik Bhattacharjee** conceptualization (lead), data curation (lead), formal analysis (lead), investigation (lead), methodology (lead), visualization (lead), writing-original draft (lead), writing-review & editing (lead); **Dayalis S. V. Brown** conceptualization (equal), data curation (equal), formal analysis (equal), writing-review & editing (equal); **Trent E. Ethridge** data curation (equal), formal analysis (equal), investigation (equal), methodology (equal), writing-review & editing (equal); **Kristine Marie Halvorsen** data curation (equal), formal analysis (equal), writing-review & editing (supporting); **Alejandra C. Acevedo Montano** data curation (supporting), formal analysis (supporting), writing-review & editing (supporting); **Theresa M. McCormick** conceptualization (equal), data curation (equal), formal analysis (equal), funding acquisition (equal), investigation (equal), methodology (equal), project administration (equal), resources (equal), supervision (equal), validation (equal), visualization (equal), writing-original draft (equal), writing-review & editing (equal).

Notes

The authors declare no competing financial interest.

■ ACKNOWLEDGMENTS

■ REFERENCES

(1) Lewis, N. S.; Nocera, D. G. Powering the Planet: Chemical Challenges in Solar Energy Utilization. *Proc. Natl. Acad. Sci. U. S. A.* **2006**, *103* (43), 15729−15735.

(2) Eisenberg, R.; Gray, H. B.; Crabtree, G. W. Addressing the Challenge of Carbon-Free Energy. *Proc. Natl. Acad. Sci. U. S. A.* **2020**, *117*, 12543−12549.

(3) Han, Z.; Eisenberg, R. Fuel from Water: The Photochemical Generation of Hydrogen from Water. *Acc. Chem. Res.* **2014**, *47* (8), 2537−2544.

(4) Mccarthy, B. D.; Dempsey, J. L. Decoding Proton-Coupled Electron Transfer with Potential - pK_a Diagrams. *Inorg. Chem.* **2017**, *56*, 1225−1231.

(5) Rountree, E. S.; Mccarthy, B. D.; Dempsey, J. L. Decoding Proton-Coupled Electron Transfer with Potential-pK_a Diagrams: Applications to Catalysis. *Inorg. Chem.* **2019**, *58*, 6647−6658.

(6) Li, C.; Baek, J. B. Recent Advances in Noble Metal (Pt, Ru, and Ir)-Based Electrocatalysts for Efficient Hydrogen Evolution Reaction. *ACS Omega.* **2020**, *5*, 31−40.

(7) Du, P.; Eisenberg, R. Catalysts Made of Earth-Abundant Elements (Co, Ni, Fe) for Water Splitting: Recent Progress and Future Challenges. *Energy Environ. Sci.* **2012**, *5* (3), 6012−6021.

(8) Han, Z.; Shen, L.; Brennessel, W. W.; Holland, P. L.; Eisenberg, R. Nickel Pyridinethiolate Complexes as Catalysts for the Light-Driven Production of Hydrogen from Aqueous Solutions in Noble-Metal-Free Systems. *J. Am. Chem. Soc.* **2013**, *135* (39), 14659−14669.

(9) Hong, D.; Tsukakoshi, Y.; Kotani, H.; Ishizuka, T.; Ohkubo, K.; Shiota, Y.; Yoshizawa, K.; Fukuzumi, S.; Kojima, T. Mechanistic Insights into Homogeneous Electrocatalytic and Photocatalytic Hydrogen Evolution Catalyzed by High-Spin Ni(II) Complexes with S_2N_2-Type Tetradentate Ligands. *Inorg. Chem.* **2018**, *57* (12), 7180−7190.

(10) Inoue, S.; Mitsuhashi, M.; Ono, T.; Yan, Y. N.; Kataoka, Y.; Handa, M.; Kawamoto, T. Photo- and Electrocatalytic Hydrogen Production Using Valence Isomers of $N_2S_2^-$-Type Nickel Complexes. *Inorg. Chem.* **2017**, *56* (20), 12129−12138.

(11) Drosou, M.; Kamatsos, F.; Mitsopoulou, C. A. Recent Advances in the Mechanisms of the Hydrogen Evolution Reaction by Non-Innocent Sulfur-Coordinating Metal Complexes. *Inorg. Chem. Front.* **2020**, *7* (1), 37−71.

(12) Zarkadoulas, A.; Field, M. J.; Artero, V.; Mitsopoulou, C. A. Proton-Reduction Reaction Catalyzed by Homoleptic Nickel - Bis-1,2-Dithiolate Complexes : Experimental and Theoretical Mechanistic Investigations. *ChemCatChem* **2017**, *9*, 2308−2317.

(13) Drosou, M.; Zarkadoulas, A.; Bethanis, K.; Mitsopoulou, C. A. Structural Modifications on Nickel Dithiolene Complexes Lead to Increased Metal Participation in the Electrocatalytic Hydrogen Evolution Mechanism. *J. Coord. Chem.* **2021**, *74* (9−10), 1425−1442.

(14) Kochem, A.; O'Hagan, M.; Wiedner, E. S.; Van Gastel, M. Combined Spectroscopic and Electrochemical Detection of a Ni(I)···H-N Bonding Interaction with Relevance to Electrocatalytic H_2 Production. *Chem. - A Eur. J.* **2015**, *21* (29), 10338−10347.

(15) James, T. L.; Cai, L.; Muetterties, M. C.; Holm, R. H. Dihydrogen Evolution by Protonation Reactions of Nickel(I). *Inorg. Chem.* **1996**, *35* (14), 4148−4161.

(16) Jacques, P. A.; Artero, V.; Pecaut, J.; Fontecave, M. Cobalt and Nickel Diimine-Dioxime Complexes as Molecular Electrocatalysts for Hydrogen Evolution with Low Overvoltages. *Proc. Natl. Acad. Sci. U. S. A.* **2009**, *106* (49), 20627−20632.

(17) Han, Z.; McNamara, W. R.; Eum, M. S.; Holland, P. L.; Eisenberg, R. A Nickel Thiolate Catalyst for the Long-Lived Photocatalytic Production of Hydrogen in a Noble-Metal-Free System. *Angew. Chemie - Int. Ed.* **2012**, *51* (7), 1667−1670.

(18) Virca, C. N.; McCormick, T. M. DFT Analysis into the Intermediates of Nickel Pyridinethiolate Catalysed Proton Reduction. *Dalt. Trans.* **2015**, *44* (32), 14333−14340.

(19) Bhattacharjee, A.; Brown, D. S. V.; Virca, C. N.; Ethridge, T. E.; Mendez Galue, O.; Pham, U. T.; McCormick, T. M. Computational Investigation into Intramolecular Hydrogen Bonding Controlling the Isomer Formation and p*Ka* of Octahedral Nickel(II) Proton Reduction Catalysts. *Dalt. Trans.* **2022**, *51* (9), 3676−3685.

(20) Virca, C. N.; Lohmolder, J. R.; Tsang, J. B.; Davis, M. M.; McCormick, T. M. Effect of Ligand Modification on the Mechanism of Electrocatalytic Hydrogen Production by Ni(Pyridinethiolate)$_3^-$ Derivatives. *J. Phys. Chem. A* **2018**, *122* (11), 3057−3065.

(21) Frisch, M. J.; Trucks, G. W.; Schlegel, H. B.; Scuseria, G. E.; Robb, M. A.; Cheeseman, J. R.; Scalmani, G.; Barone, V.; Mennucci, B.; Petersson, G. A.; Nakatsuji, H.; Caricato, M.; Li, X.; Hratchian, H. P.; Izmaylov, A. F.; Bloino, J.; Zheng, G.; Sonnenb, D. J. *Gaussian 09*, Revision D; Gaussian, Inc.: Wallingford, CT, 2009.

(22) Solis, B. H.; Hammes-Schiffer, S. Proton-Coupled Electron Transfer in Molecular Electrocatalysis: Theoretical Methods and Design Principles. *Inorg. Chem.* **2014**, *53* (13), 6427−6443.

(23) Cramer, C. J.; Truhlar, D. G. Density Functional Theory for Transition Metals and Transition Metal Chemistry. *Phys. Chem. Chem. Phys.* **2009**, *11* (46), 10757−10816.

(24) Marenich, A. V.; Ho, J.; Coote, M. L.; Cramer, C. J.; Truhlar, D. G. Computational Electrochemistry: Prediction of Liquid-Phase Reduction Potentials. *Phys. Chem. Chem. Phys.* **2014**, *16* (29), 15068−15106.

(25) Liao, R. Z.; Siegbahn, P. E. M. Quantum Chemical Modeling of Homogeneous Water Oxidation Catalysis. *ChemSusChem* **2017**, *10* (22), 4236−4263.

(26) Himmel, D.; Radtke, V.; Butschke, B.; Krossing, I. Basic Remarks on Acidity. *Angew. Chemie - Int. Ed.* **2018**, *57* (16), 4386−4411.

(27) Grzelak, I.; Orwat, B.; Kownacki, I.; Hoffmann, M. Quantum-Chemical Studies of Homoleptic Iridium(III)Complexes in OLEDs: *Fac* versus *Mer* Isomers. *J. Mol. Model.* **2019**, *25* (154), 2−9.

(28) Dennington, R.; Keith, T. A.; Millam, J. M. *GaussView*, Version 5; Semichem Inc.: Shawnee Mission, KS, 2016.

(29) Bader, R. F. W. A Quantum Theory of Molecular Structure and Its Applications. *Chem. Rev.* **1991**, *91* (5), 893−928.

(30) Bader, R. F. W. *Atoms in Molecules: A Quantum Theory*; Oxford University Press: New York, 1994.

(31) Kumar, P. S. V.; Raghavendra, V.; Subramanian, V. Bader's Theory of Atoms in Molecules (AIM) and Its Applications. *J. Chem. Sci.* **2016**, *128* (10), 1527−1536.

(32) Lu, T.; Chen, F. Multiwfn: A Multifunctional Wavefunction Analyzer. *J. Comput. Chem.* **2012**, *33* (5), 580−592.

(33) Spackman, M. A. Hydrogen Bond Energetics from Topological Analysis of Experimental Electron Densities: Recognising the Importance of the Promolecule. *Chem. Phys. Lett.* **1999**, *301* (5−6), 425−429.

(34) Emamian, S.; Lu, T.; Kruse, H.; Emamian, H. Exploring Nature and Predicting Strength of Hydrogen Bonds: A Correlation Analysis Between Atoms-in-Molecules Descriptors, Binding Energies, and Energy Components of Symmetry-Adapted Perturbation Theory. *J. Comput. Chem.* **2019**, *40* (32), 2868−2881.

(35) Addison, A. W.; Rao, T. N.; Reedijk, J.; van Rijn, J.; Verschoor, G. C. Synthesis, Structure, and Spectroscopic Properties of Copper-(II) Compounds Containing Nitrogen-Sulphur Donor Ligands; the Crystal and Molecular Structure of Aqua[1,7-Bis(*N*-Methylbenzimi-dazol-2'-yl)-2,6-Dithiaheptane]Copper(II). *J. Chem. Soc. Dalt. Trans.* **1984**, *3*, 1349−1356.

(36) Crans, D. C.; Tarlton, M. L.; Mclauchlan, C. C. Trigonal Bipyramidal or Square Pyramidal Coordination Geometry? Investigating the Most Potent Geometry for Vanadium Phosphatase Inhibitors. *Eur. J. Inorg. Chem.* **2014**, *2014*, 4450−4468.

(37) Kelly, C. P.; Cramer, C. J.; Truhlar, D. G. Single-Ion Solvation Free Energies and the Normal Hydrogen Electrode Potential in Methanol, Acetonitrile, and Dimethyl Sulfoxide. *Phys. Chem. B* **2007**, *111*, 408−422.

(38) Zhan, C. G.; Dixon, D. A. The Nature and Absolute Hydration Free Energy of the Solvated Electron in Water. *J. Phys. Chem. B* **2003**, *107* (18), 4403−4417.

(39) Grills, D. C.; Lymar, S. V. Solvated Electron in Acetonitrile: Radiation Yield, Absorption Spectrum, and Equilibrium between Cavity- and Solvent-Localized States. *J. Phys. Chem. B* **2022**, *126* (1), 262−269.

(40) Marković, Z.; Tošović, J.; Milenković, D.; Marković, S. Revisiting the Solvation Enthalpies and Free Energies of the Proton and Electron in Various Solvents. *Comput. Theor. Chem.* **2016**, *1077*, 11−17.